J Mater Sci (2020) 55:7702–7714

Electronic materials

Enhanced H_2S gas sensing properties by the optimization of p-CuO/n-ZnO composite nanofibers

Chao Fan[1,2], Fazhe Sun[3], Xiaomei Wang[2,*], Mahyar Majidi[2], Zuzhen Huang[2], Parveen Kumar[2], and Bo Liu[1,2,*]

[1] School of Materials Science and Engineering, Shandong University of Technology, Zibo 255049, Shandong, People's Republic of China

[2] Laboratory of Functional Molecules and Materials, School of Physics and Optoelectronic Engineering, Shandong University of Technology, Zibo 255049, Shandong, People's Republic of China

[3] Analysis and Testing Center, Shandong University of Technology, Zibo 255049, Shandong, People's Republic of China

Received: 1 October 2019
Accepted: 24 December 2019
Published online: 26 March 2020

ABSTRACT

Recently, metal oxide nanomaterials-based gas sensors have been widely applied in the detection of hydrogen sulfide (H_2S). In this work, the optimal composition of CuO and ZnO in CuO/ZnO nanofibers (CZ NFs) gas sensor to improve its gas sensing performances has been first proposed. In this work, pure CuO NFs and CZ composite NFs with different molar ratios were prepared by the facile electrospinning method. A series of detection was carried out to examine the gas sensing performances of pure CuO NFs and CZ NFs. The results indicated that the CZ4 (CuO/ZnO = 1:2) NFs sensor achieved the highest response (31.472 ± 0.7997) toward 50 ppm H_2S gas at 180 °C compared with other sensors fabricated in this experiment. The gas sensing mechanism of pure CuO and CZ NFs sensors was described in detail. The results indicated that the H_2S sensing performances of CZ NFs could be effectively improved by optimizing the composition of CZ NFs. Furthermore, the p–n junctions between ZnO and CuO in the CZ NFs also played an important role to enhance the response of CZ composites NFs toward H_2S.

Introduction

Hydrogen sulfide (H_2S) is a flammable, colorless, and toxic gas having rotten eggs smell [1, 2]. Low concentration exposure of H_2S for a long time could cause headache, dizziness, and irritation in eyes and nasal cavity, whereas exposure in a high concentration could result in acute poisoning or even death [3, 4]. Therefore, the development of an efficient sensor to monitor harmful H_2S gas is an important research topic. A large number of sensors were

Address correspondence to E-mail: xiaomeiwang@sdut.edu.cn; liub@sdut.edu.cn

https://doi.org/10.1007/s10853-020-04569-8

applied in monitoring H_2S gas including optical [5], electrochemical [6], and semiconducting oxide [7, 8] sensors. In terms of the sensitivity of optic and semiconductor sensors, both of the two sensors could detect the sub-ppm concentration of H_2S gas [9–11]. Optical sensors possess the characteristics of high sensitivity and accuracy [12] and their sensing materials included metal oxide materials [13] and polymers [14], but the equipment for the optical sensors is expensive and complicated to operate which hinders their development. Electrochemical sensors are suitable for mass production, but their sensitivity could easily be affected by the environment [15]. By contrast, semiconducting oxide sensors have many advantages such as low cost, facile operation, and small size compared with other sensors. The sensing materials of semiconducting oxide sensors mainly include semiconductor oxides such as ZnO [16, 17], SnO_2 [18–22], In_2O_3 [23, 24], WO_3 [25], etc.

High gas sensitivity and selectivity, fast response speed and short recovery time are necessary parameters of excellent gas sensors. These characteristics are difficult to achieve with only one type of semiconducting metal oxide material [26–29]. The traditional way to enhance gas sensing performances was doping with metal such as (Co, Ag, Pd, Au, and Ni) to form Co–ZnO [30], Ag–ZnO [31], Pd–ZnO [32], Au–ZnO [33], Ni–ZnO [34], etc. The construction of heterostructure such as ZnO/SnO_2 [35–37], NiO/ZnO [38, 39], ZnO/$ZnFe_2O_4$ [40], Cr_2O_3/SnO_2 [41], etc., has become a novel and popular direction to improve the gas sensing performance. Among these oxides, ZnO has become the most popular research object due to its wide bandgap (3.37 eV), outstanding chemical and thermal stability, and large exciton binding energy (60 meV) [42–44]. CuO as a typical p-type oxide has the lowest enthalpy change [45], and its surface has the strongest oxygen adsorption capacity [46]. The combination of CuO and ZnO can promote the change of conductance and improve the gas sensitivity of materials [47, 48]. Moreover, many researchers proved that the formation of p-CuO/n-ZnO heterojunctions could effectively improve gas sensing performance. Zhang et al. reported the high ethanol(C_2H_5OH) sensing properties of p-CuO/n-ZnO heterojunction flower structure nanorods, which probably related to the formation of p–n heterojunctions [49]. Diao et al. fabricated ZnO/CuO core–shell nanowires-based gas sensors and investigated the performance toward NO_2 and benzene in which the p–n junctions of the sensor accelerated the charge transfer to absorb the target gases [50].

What is more notable is that p-CuO/n-ZnO heterojunctions also exhibit excellent H_2S sensing performance. Liu et al. fabricated the CuO NP-capped ZnO nanorods by physical layer deposition (PLD) method which exhibited high selectivity toward hydrogen disulfide (H_2S) at room temperature [51]. Li et al. synthesized the rough nanotubular arrays by ultrasonic spray pyrolysis (USP) and chemical bath deposition (CBD) method which showed the high H_2S sensing properties at low-working temperatures [52]. Katoch et al. prepared ZnO/CuO nanofibers (NFs) with various nanograin sizes by changing the heat treatment duration in which the smaller nanograins samples showed the superior sensitivity for H_2S compared with larger nanograins [53]. Optimization of composite NFs ratio is a simple and effective way to enhance the gas sensing properties of the material [54–56]. However, optimization of the ratio of CuO/ZnO NFs (CZ NFs) to improve its gas sensing performance toward H_2S gas has been rarely reported. In this work, in order to construct CZ NFs and optimize its gas sensing properties, five kinds of CZ NFs (with different ratios of ZnO and CuO) and pure CuO NFs were synthesized by electrospinning and subsequent calcination method. The CZ NFs-based gas sensor showed superior sensing performances compared with pure CuO NFs-based gas sensor. Moreover, the CZ4 NFs (CuO/ZnO; 1:2) exhibited the best sensing properties toward H_2S gas compared with other CZ NFs. In addition, the sensing mechanism of the pure CuO NFs and CZ NFs gas sensors has been proposed in detail. In our opinion, p–n heterojunctions between ZnO and CuO could be beneficial in enhancing the gas sensing properties of CZ NFs sensors.

Experimental

Materials

Copper acetate monohydrate ($Cu(CH_3COO)_2{\cdot}H_2O$), zinc acetate dihydrate ($Zn(CH_3COO){\cdot}2H_2O$), polyvinylpyrrolidone (PVP) (M_w = 1300000), absolute ethanol (C_2H_5OH) and *N*, *N*-Dimethylformamide (DMF) were purchased from Sinopharm Chemical Reagent Co., Ltd. All the chemicals reagents were of

analytical grade and used without any further purification.

Synthesis of pure CuO and CuO/ZnO composite NFs

Five kinds of precursor solutions were prepared with a different molar ratio of Cu^{2+} and Zn^{2+} (3:1, 2:1, 1:1, 1:2, and 1:3, marked as CZ1, CZ2, CZ3, CZ4, and CZ5, respectively). The specific procedure was divided into two steps. Firstly, $Cu(CH_3COO)_2{\cdot}H_2O$ and $Zn(CH_3COO){\cdot}2H_2O$ were dissolved in a mixed solution of 10 mL absolute ethanol and 10 mL DMF and stirred for 15 min. After that, 2 g PVP was slowly added and continued stirring for 10 h to obtain a uniform precursor solution. For preparing CuO NFs, only $Cu(CH_3COO)_2{\cdot}H_2O$ was used and 2.3659 g of PVP added according to the above-described procedure. In the electrospinning process, the precursor solutions were filled into a plastic syringe with a capacity of 10 mL. The distance between the syringe needle (inner diameter = 0.34 mm) and the collecting substrate (aluminum foil) was adjusted to 15 cm. A positive voltage (+ 9 kV) was applied to the needle to provide a high voltage electrical field, and a negative voltage (− 2 kV) was applied to the aluminum foil to remove static electricity. The feeding rate of the precursor solution was kept at a constant rate of 0.56 mL/h by a syringe pump. Herein, all the solutions were injected within 12 h. The thickness of obtained precursor NFs was measured to be 28 μm (Fig S1). Finally, the precursor NFs were sintered at 500 °C for 4 h in the air to obtain the respective pure CuO NFs and CZ NFs. Figure 1 shows the electrospinning step and the calcination process used for the preparation of CZ NFs.

Gas sensors fabrication and sensitivity evaluation

Gas sensors were produced by a screen-printing method. First, 0.05 g CZ NFs were mixed with 100 μL absolute ethanol in an agate mortar to obtain a uniform paste. Then, the obtained paste was placed on the plate and the press plate was used to print the paste onto the underlying electrode sheet. The concrete structure of the screen-printing device is shown in Fig. 2. The fabricated gas sensors were dried at room temperature for 24 h. Then, the sensors were sintered at 500 °C for 24 h to improve stability before the gas sensing tests. The gas sensing properties of sensors were tested on a CGS-4TP intelligent gas sensing analysis system (Beijing Elite Tech Co. Ltd., China). In the gas sensing process, different concentrations of target gases were injected into the 1.8 L test chamber using microsyringe. The response value is defined as R = Ra/Rg. Here, Ra is the resistance of gas sensors after stabilization in the air atmosphere and Rg is the resistance of gas sensors after injecting target gases. The time of the sensors to obtain 90% of the full response and reduced to 10% of the maximum response was marked as the response and recovery time, respectively.

Materials characterization

The phase compositions of the pure CuO NFs and CZ NFs were measured by X-ray diffraction (XRD, D8-Advance) with Cu Kα radiation (λ = 1.5405 Å). The surface morphology of the pure CuO NFs and CZ NFs was characterized by a scanning electron microscope (SEM, FEI Sirion 200F). Transmission electron microscopy (TEM), high-resolution transmission electron microscopy (HRTEM), and selected area electron diffractive (SAED) results were obtained on FEI Tecnai G2 F20 S-TWIN. The energy dispersive spectra (EDS) were measured by the SEM attachment.

Results and discussion

Characterizations of the electrospun pure CuO NFs and CZ NFs

Figure 3 displays the X-ray diffraction (XRD) graphs of pure CuO, CZ1, CZ2, CZ3, CZ4, and CZ5 NFs. The patterns showed that diffraction peaks located at 2θ = 31.89°, 34.54°, 36.37°, 47.67°, 56.72°, 62.99°, 68.09°, and 69.18° were well indexed to the (100), (002), (101), (102), (110), (103), (112), and (201) crystal planes of hexagonal wurtzite ZnO, respectively (JCPDS Card NO.36-1451). Other diffraction peaks located at 2θ = 32.58°, 35.57°, 38.77°, 48.85°, 53.48°, 58.31°, 61.59°, 66.31°, 68.05°, 72.45°, and 75.08° correspond to the (110), (11-1), (111), (20-2), (020), (202), (11-3), (31-1), (220), (311), and (22-2) crystal planes of monoclinic CuO, respectively (JCPDS Card No.48-1548). Pure CuO NFs did not show any diffraction peak of ZnO (curve a) and CZ1, CZ2 and CZ3 (curve

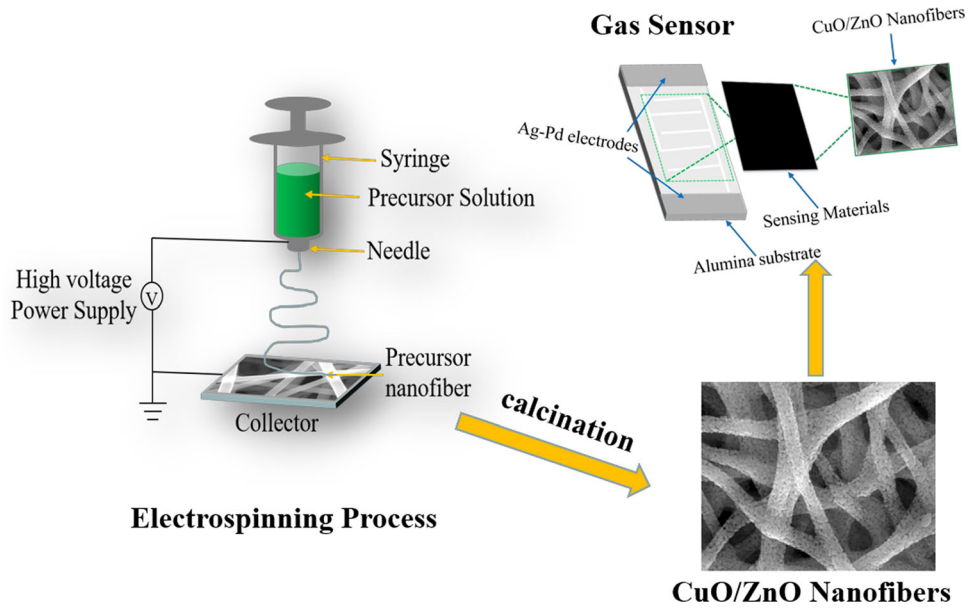

Figure 1 The schematic diagram of CuO/ZnO NFs synthesis and the structure of the gas sensor.

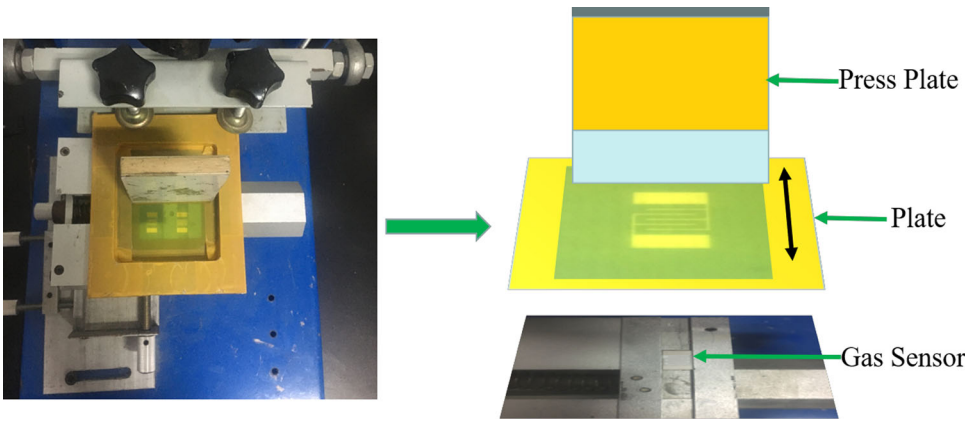

Figure 2 The schematic diagram of the screen-printing device.

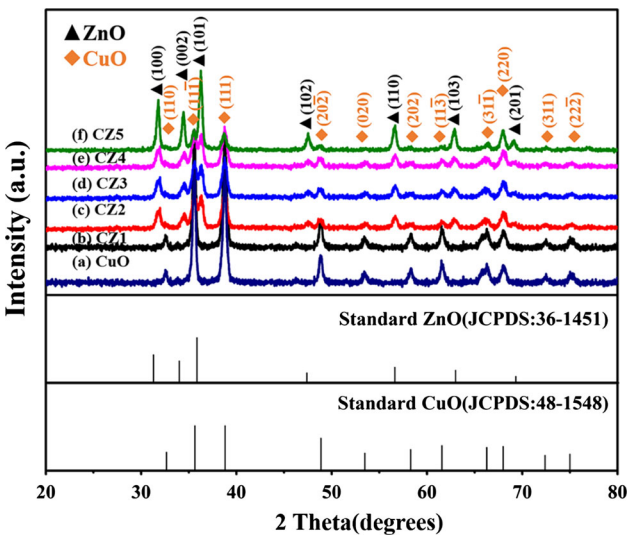

Figure 3 XRD patterns of pure CuO NFs and CZ NFs.

b–d) NFs exhibited small diffraction peaks of ZnO, suggesting the less ZnO content in these materials compared to other materials. It can be concluded from the XRD patterns that with increasing CuO content in the CZ NFs, the intensity of the CuO characteristic peaks increased. No impurity peaks appeared in the XRD patterns, indicating high purity of pure CuO NFs and CZ NFs. The XRD patterns also confirmed that CZ NFs contain separate phases of ZnO and CuO, which can promote the p–n hetero-junctions generated between the ZnO and CuO interface. The XRD patterns estimated that the pre-cursor NFs in calcination at 500 °C for 4 h were adequate to remove PVP and to form the highly crystalline CZ NFs.

The crystallite size (D) of CuO and ZnO phases was estimated using Scherrer's formula,

$$D = \frac{0.9\lambda}{\beta \cos\theta} \quad (1)$$

where λ represents the wavelength of the X-radiation (λ = 1.5405 Å), β represents the full width at half maximum (FWHM) of the highest intense peak and θ represents the diffraction angle of the radiation. The crystallite size of CuO and ZnO phases was calculated using (11-1) and (101) planes, respectively. The lattice parameters of CuO and ZnO were estimated using Eqs. (2) and (3), respectively.

$$\frac{1}{d^2} = \left(\frac{h^2}{a^2} + \frac{k^2}{a^2}\right) + \left(\frac{l^2}{c^2}\right) \quad (2)$$

$$\frac{1}{d^2} = \frac{1}{sin^2\beta}\left(\frac{h^2}{a^2} + \frac{k^2 sin^2\beta}{b^2} + \frac{l^2}{c^2} - \frac{2hl\cos\beta}{ac}\right) \quad (3)$$

The crystallite sizes of the CuO phase of CuO NFs were found to be 23 nm. The crystallite sizes of the CuO phase of CZ NFs were found to be in the range of 18–27 nm, and the ZnO phase was determined to be between 12 and 22 nm. Lattice constants of CuO and ZnO are summarized in Table 1. It can be seen from Table 1 that the lattice constants of CuO and CZ NFs have some crystal distortions compared with the standard value (a = 4.685 Å, b = 3.425 Å, and c = 5.130 Å).

SEM image of the precursor CuO NFs showed a uniform diameter and smooth surface (Fig. 4a). Figure 4b shows that the obtained CuO material was composed of uniform NPs with an average diameter of approximately 115 nm. By measurement, the diameter of most of the NPs was found to be in the range of 80–120 nm.

Figure 5a–e displays the SEM morphology of five proportions precursor CZ NFs (the insets) and calcined CZ NFs. All the precursor CZ NFs were smooth with uniform length diameter as shown in the insets. CZ NFs were composed with a lot of nanograins via crystal growth during annealing and formed nanogaps in the NFs due to the removal of organic polymers and solvents. Figure 5d shows that the nanograins of CZ4 were more uniform and contained more gaps between nanograins than other samples. The elemental composition of CZ4 NFs was observed through the TEM-EDS mappings (Fig. 5f). The mapping image displayed that the Cu, Zn, and O elements were well scattered on CZ NFs confirming that CZ NFs contained ZnO and CuO phases. The average diameters of the precursor CZ NFs were about 603 ± 43 nm (CZ1), 595 ± 51 nm (CZ2), 601 ± 49 nm (CZ3), 589 ± 44 nm (CZ4), and 588 ± 64 nm (CZ5). The average diameters of most precursor CZ NFs were found to be in the range of 600–650 nm. The CZ3 NFs exhibited the smallest average diameter (288 ± 46 nm), whereas the CZ1 NFs exhibited the largest average diameter (429 ± 82 nm). However, the average diameters of the other three CZ NFs were 423 ± 66 nm (CZ2), 399 ± 88 nm (CZ4), and 349 ± 80 nm (CZ5). Compared with the precursor CZ NFs, the diameter of CZ NFs was significantly reduced due to the removal of the polymers after calcination.

Figure 6a shows a low-magnification TEM image of CZ4 NFs and inset shows the whole CZ4 NFs. It could be clearly seen that the CZ4 NFs were composed of NPs in which the darker ones were CuO NPs. However, the average sizes of ZnO NPs and CuO NPs were less than 100 nm. Figure 6b displays a more high-resolution TEM image of CZ NFs. Two interplanar distances in the CZ4 NF were 0.2476 nm and 0.2752 nm, which can be indexed to (101) lattice plane of hexagonal wurtzite ZnO, and (111) crystal plane of monoclinic CuO, respectively. The lattice distortion between CuO and ZnO interfaces was

Table 1 The lattice parameters and crystallite sizes of pure CuO NFs and CZ NFs

Samples	ZnO		CuO			Crystallite size (nm)	
	Hexagonal (ZnO 36-1451)		Monoclinic (CuO 48-1548)			ZnO	CuO
	Lattice parameters (Å)		Lattice parameters (Å)				
	a	*c*	*a*	*b*	*c*		
CuO	–	–	4.6322	3.4250	5.1879	–	23
CZ1	3.2493	5.1606	4.6589	3.4341	5.2127	12	27
CZ2	3.2456	5.1609	4.6581	3.4353	5.1889	13	24
CZ3	3.2423	5.2133	4.6651	3.4256	5.1876	17	21
CZ4	3.2411	5.1932	4.6323	3.4335	5.2136	20	19
CZ5	3.2483	5.2176	4.6599	3.4346	5.1982	22	18

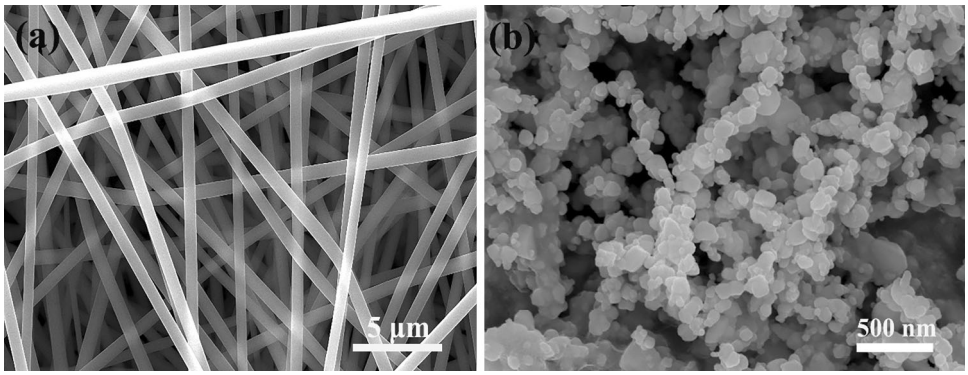

Figure 4 SEM micrographs of **a** precursor CuO NFs **b** pure CuO.

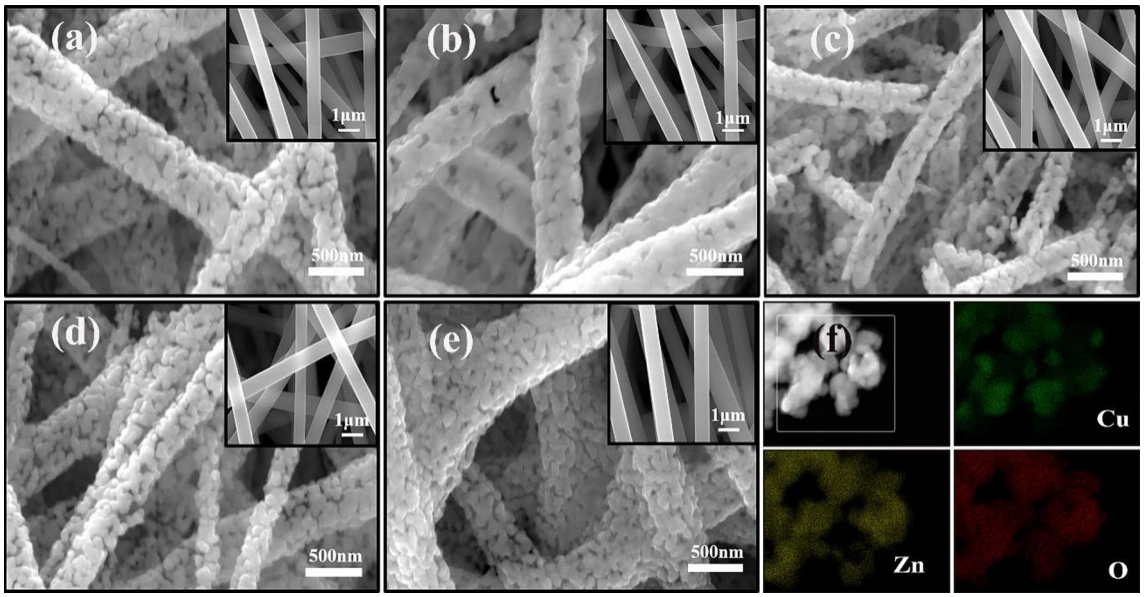

Figure 5 SEM micrographs of **a** CZ1, **b** CZ2, **c** CZ3, **d** CZ4, **e** CZ5 NFs. The insets in these figures show low-magnification SEM images of the corresponding precursor CZ NFs, **f** TEM-EDS elemental mapping scan of the CZ4 NFs.

noticed which are labeled by yellow lines in the red oval. In addition, the interface difference can be clearly seen in the upper area of the TEM image (Fig. 6b) which confirmed the existence of p–n heterojunctions inside the CZ NFs. The SAED (selected area electron diffraction) pattern showed a polycrystalline phase of the CZ4 NFs. The distributed bright diffraction spots confirmed that the NFs were composed of ZnO NPs and CuO NPs which was also confirmed by the EDS spectra. As shown in Fig. 6d, the weight percentage of oxygen, copper, and zinc in these materials was computed to be about 24.20, 25.06, and 50.74, respectively. The weight and atomic percentage ratio of the Cu to Zn were approximately 1:2 in all the cases which were consistent with the theoretical value. Thus, it proves the uniform composition of CuO/ZnO within the NFs. Meanwhile, the atomic percentage of oxygen, copper, and zinc in these materials was calculated to be about 54.11, 15.25, and 30.64, respectively. The ratios of Cu^{2+} and Zn^{2+} were in good agreement with the precursor solution. The results indicated the formation of ZnO/CuO heterojunctions which could enhance the performance of gas sensing. Furthermore, the results of the TEM were well consistent with the XRD pattern.

Gas sensing performances of the pure CuO NFs and CZ NFs

Gas sensing tests of pure CuO NFs and CZ NFs-based gas sensors

Since the operating temperature is an important working parameter of gas sensors, the sensing performances of gas sensors toward H_2S were

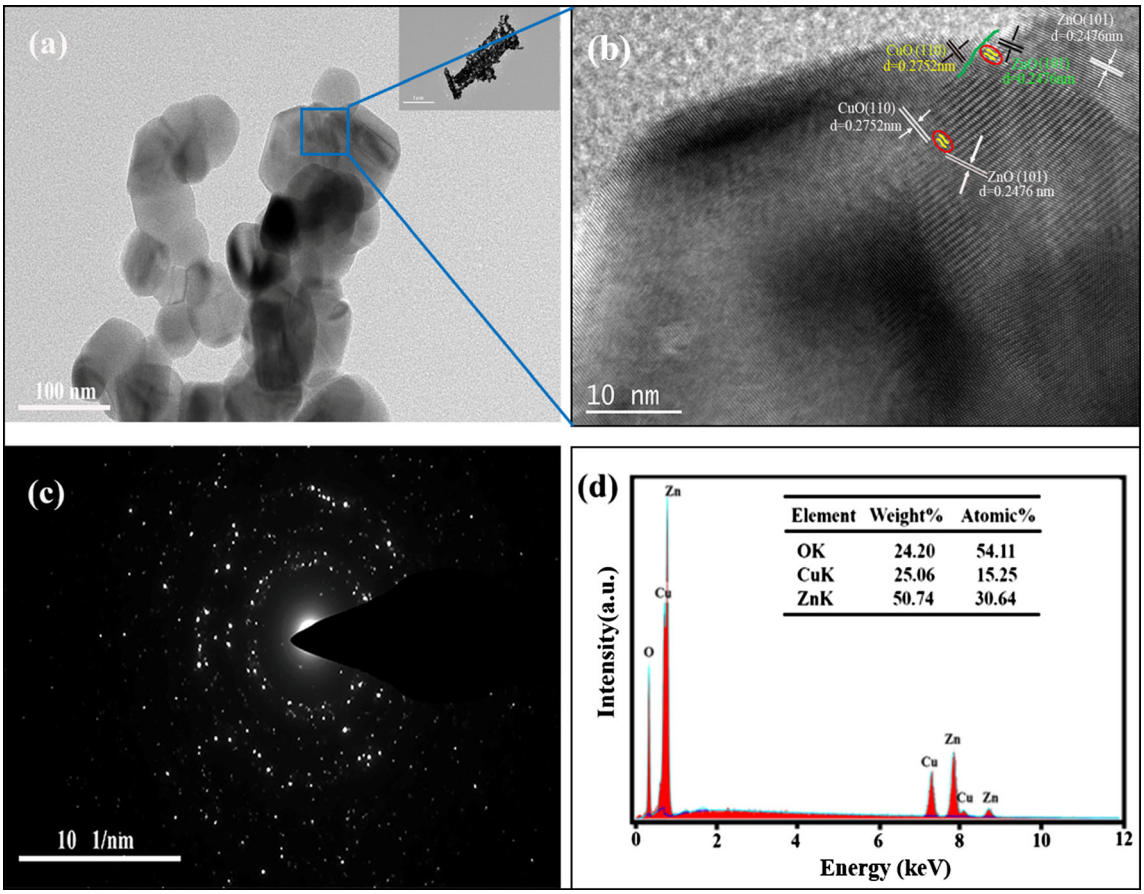

Figure 6 **a** Low-magnification TEM images of CZ4 NFs. The inset is the whole CZ4 NFs, **b** high-magnification TEM images of CZ4 NFs, **c** the corresponding SAED pattern, **d** EDS spectra of CZ4 NFs.

investigated at different temperatures. Figure 7a shows the response of gas sensors at the operating temperatures ranging from 150 to 270 °C toward 50 ppm H_2S gas. All CZ NFs sensors achieved the maximum response toward H_2S at 180 °C, while the pure CuO NFs sensor attained the maximum response toward H_2S at 210 °C. Therefore, further gas sensing tests toward H_2S were carried out at 180 °C.

Similarly, selectivity is an important gas sensing parameter. Hence, gas sensing tests of pure CuO NFs and CZ NFs sensors toward various gases such as acetone (CH_3COCH_3), formaldehyde (CH_2O), methanol (CH_3OH), acetic acid (CH_3COOH), ethanol and H_2S were carried out.

The responses of pure CuO NFs and CZ NFs gas sensors toward 50 ppm H_2S and 100 ppm other gases are shown in Fig. 7b. The response of H_2S gas was detected at an operating temperature of 180 °C, whereas responses of other target gases were detected from 150 to 390 °C to obtain the optimal response. The CZ4 NFs gas sensor showed the highest selectivity toward 50 ppm H_2S with a response value of 31.472 ± 0.7997. The response and recovery curves of pure CuO NFs and CZ NFs gas sensors to 50 ppm H_2S are illustrated in Fig. 7c. The response and recovery times of the CZ4 NFs gas sensor to 50 ppm H_2S were about 134.5 s and 182 s, respectively. Response and recovery times of other samples were CuO NFs (20/90 s), CZ1 NFs (155/136 s), CZ2 NFs (126/105 s), CZ3 NFs (195/107 s), and CZ5 NFs (105/152 s). Similarly, the sensitivities of sensors to various concentrations of H_2S gas are displayed in Fig. 7d. Because H_2S gas is extremely toxic at low concentrations and the limit of H_2S gas detection of each sensor was 1 ppm after many repeated tests, therefore the detection range was set from 1 to 50 ppm. On increasing the concentration of H_2S gas, the sensitivities of the CZ4 and CZ5 NFs sensors increased rapidly, while the responses of the other sensors did not change significantly. In contrast, the pure CuO

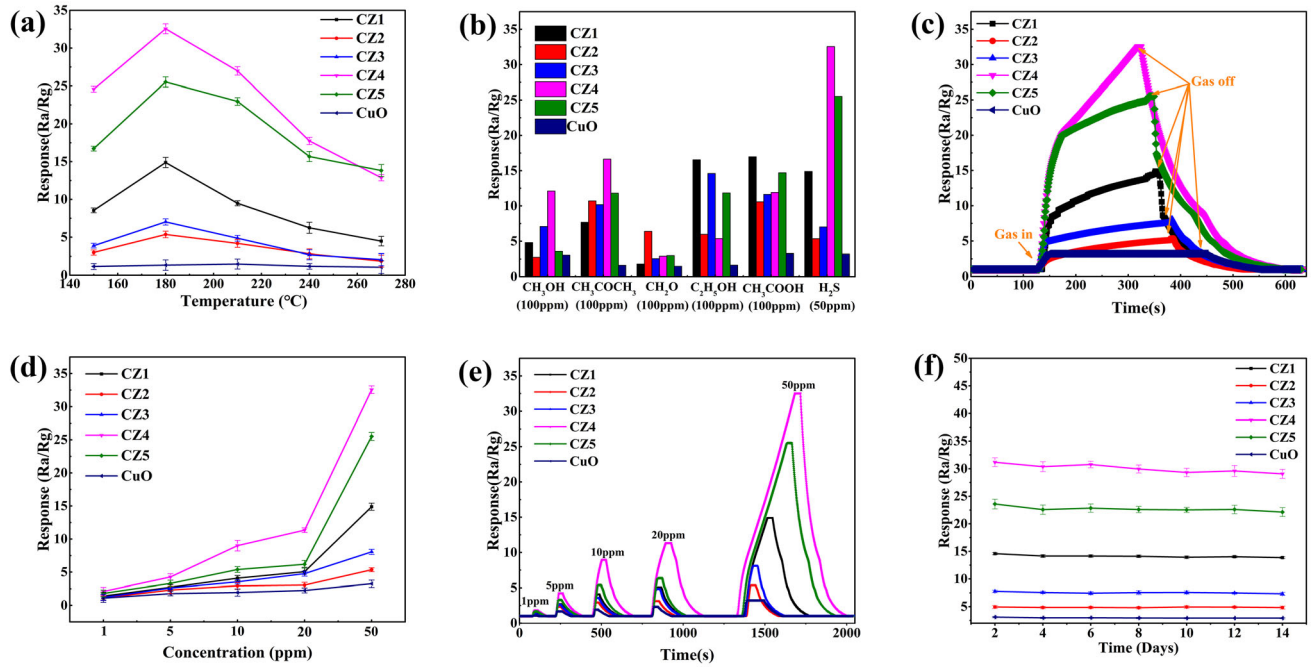

Figure 7 **a** Response–recovery curves of pure CuO NFs and CZ NFs gas sensors toward H_2S gas at different operating temperatures, **b** responses of pure CuO NFs and CZ NFs gas sensors to different gases (H_2S (50 ppm) and other gases (100 ppm)) at optimum temperature, **c** response–recovery curves of pure CuO NFs and CZ NFs sensors toward 50 ppm H_2S gas, **d** the response value on H_2S gas concentration at 180 °C, **e** response–recovery curves of pure CuO and CZ NFs sensors toward H_2S gas in the concentration range of 1–50 ppm at 180 °C and **f** response of pure CuO and CZ NFs gas sensors toward 50 ppm H_2S gas at 180 °C up to 2 weeks.

NFs sensor showed the lowest response compared with other sensors. As the concentration of H_2S gas increased, the response of pure CuO NFs sensor exhibited a minor change. Meanwhile, the recovery time of the CuO NFs sensor increased with an increasing concentration of H_2S gas. Figure 7e shows the response and recovery transient graphs of all CZ NFs gas sensors to different concentrations of H_2S gas from 1 to 50 ppm. The CZ4 NFs sensor exhibited the best response value and selectivity toward H_2S gas, which holds the potential as an effective gas sensor for H_2S gas detection. It is worth noticing that the CZ4 NFs and CZ5 NFs sensors showed high selectivity to H_2S gas, while the selectivity of other samples to various gases was low. In addition, the response of pure CuO NFs sensor to different gases was relatively low. Therefore, the CZ4 NFs and CZ5 NFs sensors are more suitable as potential H_2S gas sensor compared with other sensors.

Generally, the gas sensors do not work well in detecting toxic gases if they only show high response but do not have good stability. Therefore, the gas sensing performance of pure CuO NFs and CZ NFs gas sensors was detected up to 2 weeks with 50 ppm H_2S gas in order to determine their stability. After several days, the gas sensitivity of the CZ4 NFs and CZ5 NFs gas sensors slightly decreased but maintained a high value even after two weeks (Fig. 7f). However, other gas sensors maintained stable gas sensitivity but possess low value.

A comparison of H_2S sensing properties of different materials sensors is summarized in Table 2. CZ4 and CZ5 NFs sensors exhibited a lower working temperature compared with other sensors. Low-working temperature is beneficial both to the life of the sensor and to reduce costs. Meanwhile, the response of CZ4 and CZ5 NFs sensors was relatively higher than other gas sensors. Many sensors also exhibited a longer response and recovery time for H_2S gas than the sensors in this work. Therefore, the gas sensors fabricated in this study have the potential for further investigation and application.

Gas sensing mechanism

The gas sensing mechanism of pure CuO NFs sensor was reported to be connected with the surface-absorbed oxygen species [9]. When the sensor is

exposed to the air atmosphere, a lot of oxygen molecules adsorb on the CuO surface and capture the electrons in the valence band (VB) to form oxygen ions such as O^{2-}, O^{-}, and O_2^{-}. After the H_2S gas is added to the gas sensing test chamber, the produced oxygen ions react with H_2S and the concentration of free electrons decreases and the resistance of CuO increases. The process can be described by following equations:

$$O_2(g) \rightarrow O_2(ads) \quad (4)$$

$$O_2(ads) + e^- \rightarrow O_2^-(ads) \quad (5)$$

$$O_2^-(ads) + e^- \rightarrow 2O^-(ads) \quad (6)$$

$$O^-(ads) + e^- \rightarrow O^{2-}(ads) \quad (7)$$

$$2H_2S(g) + 3O_2^-(ads) \rightarrow 2H_2O(g) + 2SO_2(g) + 3e^- \quad (8)$$

The sensing mechanism of the CZ NFs gas sensors toward H_2S not only connects with the surface-absorbed oxygen species but also relates to the formation of p–n heterojunctions. The contact between n-type ZnO and p-type CuO causes the formation of heterojunction. In the system of p–n heterojunctions, the electrons transfer from ZnO to CuO and the holes on the surface of CuO move from CuO to ZnO resulting in the formation of the depletion layer and the bend of the energy band.

When the gas sensor is exposed to air for several minutes, the depletion layer gets widen due to the transfer of electrons, as shown in Fig. 8 [62, 63]. Below 220 °C operating temperature, CuO changes to CuS in the H_2S atmosphere. In addition, above 220 °C operating temperature, CuO reacts with H_2S to form Cu_2S due to the instability of the CuS. Once the H_2S is removed from the system, CuS gets converted into CuO. The specific process can be expressed by the following Eqs. (9) and (10).

$$CuO(s) + H_2S(g) \rightarrow CuS(s) + H_2O(g) \quad (9)$$

$$2CuS(s) + 3O_2(g) \rightarrow 2CuO(s) + 2SO_2(g) \quad (10)$$

The role of p–n heterojunctions is primarily reflected in enhancing the gas sensing properties of CZ NFs sensors by accelerating the charge transfer. As the oxygen molecules adsorb onto the surface of the CZ NFs for a period of time, the resistance of sensors gets a stable value. Once the H_2S gas is introduced into the testing atmosphere, it reacts with the oxygen molecules and releases lots of electrons back to the VB [64].

The performance of gas sensing was also related to the structure of the CZ NFs. The CZ4 NFs were composed of more uniform and fine NPs than other CZ NFs. Moreover, it contained more gaps between the NPs than other CZ NFs as confirmed by the SEM. Such morphology provides many active sites for sensing reaction and gas adsorption. Therefore, more oxygen could be converted into chemisorbed oxygen which could help to improve the gas sensing performance [65]. Thus, the response not only depends on the number of p–n junctions but also the morphology of the NFs, such as the grain size and microstructures of sensing materials. Samples with smaller nanograin sizes possess higher H_2S sensing properties due to the presence of more p–n junctions than lager nanograins [53, 66, 67]. In addition, the reaction speed of target gas with sensing materials could be increased by increasing the reaction area by adjusting the microstructure of materials [68, 69].

Table 2 A comparison of H_2S sensing performances of different materials sensors reported in other literature and in this work

Sensing materials	H_2S concentration (ppm)	Working temperature (°C)	Response	Response/recovery time (s)	References
CuO nanoparticle decorated ZnO nanorod	100	100	39	120/long	Wang et al. [57]
CuO/NiO nanowall	100	260	47.6	18/29	Wang et al. [4]
CuO–WO_3 nanowires	100	300	6.72	–/–	Park et al. [58]
Pd–CuO nanorods	100	300	4	690/80	Kim et al. [59]
ZnO nanosheet	100	70	23	252/3697	Wang et al. [60]
ZnO flower	100	300	9	5/8	Guoa et al. [61]
CZ4 NFs	50	180	31.172 ± 0.7997	195/107	This work
CZ5 NFs	50	180	23.5894 ± 0.87411	105/152	This work

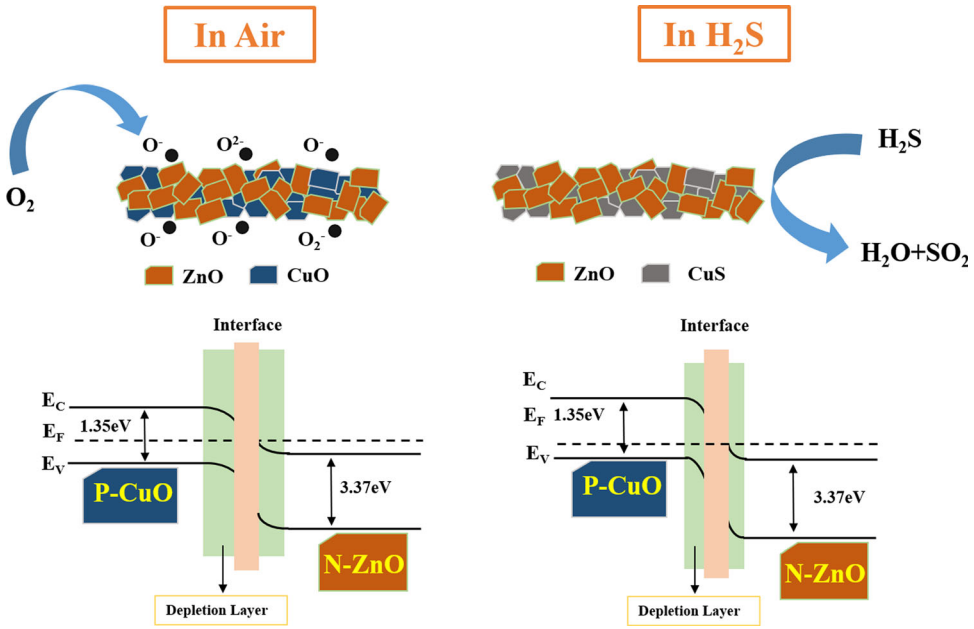

Figure 8 The sensing mechanism of the CZ NFs gas sensors in the air and H_2S gas.

Conclusions

Pure CuO NFs and five composite CuO/ZnO NFs were prepared by facile electrospinning and subsequent calcination method. A series of characterization methods have been used for composition and structural analysis. SEM showed that the CZ NFs were composed of nanograins making nanogaps in the NFs. EDS confirmed the presence of ZnO and CuO, whereas XRD confirmed the existence of ZnO and CuO in CZ NFs. Further, TEM showed that CZ NFs were composed of ZnO and CuO NPs. All the CZ NFs sensors exhibited a higher response toward H_2S gas compared with the pure CuO NFs. The sensor fabricated by CZ4 NFs achieved the highest response of 31.472 ± 0.7997 toward 50 ppm H_2S at a low temperature of 180 °C. All the results indicate that the CZ4 NFs sensor is capable of detecting H_2S gas to act as a potential gas sensing material.

Acknowledgements

The authors acknowledge the support from the National Natural Science Foundation of China (Grant Number 61704098) and the Natural Science Foundation of Shandong Province (ZR2017BF025).

Electronic supplementary material: The online version of this article (https://doi.org/10.1007/s10853-020-04569-8) contains supplementary material, which is available to authorized users.

References

[1] Kim J-H, Mirzaei A, Zheng Y, Lee J-H, Kim J-Y, Kim HW, Kim SS (2019) Enhancement of H_2S sensing performance of p-CuO nanofibers by loading p-reduced graphene oxide nanosheets. Sens Actuators B Chem 281:453–461

[2] He M, Xie L, Zhao X, Hu X, Li S, Zhu Z-G (2019) Highly sensitive and selective H_2S gas sensors based on flower-like WO_3/CuO composites operating at low/room temperature. J Alloys Compd 788:36–43

[3] Han C, Li X, Shao C, Li X, Ma J, Zhang X, Liu Y (2019) Composition-controllable p-CuO/n-ZnO hollow nanofibers for high-performance H_2S detection. Sens Actuators B Chem 285:495–503

[4] Wang Y, Qu F, Liu J, Wang Y, Zhou J, Ruan S (2015) Enhanced H_2S sensing characteristics of CuO–NiO core-shell microspheres sensors. Sens Actuators B Chem 209:515–523

[5] Zhou H, Wen J-Q, Zhang X-Z, Wang W, Feng D-Q, Wang Q, Jia F (2014) Study on fiber-optic hydrogen sulfide gas sensor. Phys Proc 56:1102–1106

[6] Wang Y, Yan H, Wang E (2002) Solid polymer electrolyte-based hydrogen sulfide sensor. Sens Actuators B Chem 87:115–121

[7] Gao C, Lin Z-D, Li N, Fu P, Wang X-H (2015) Preparation and H_2S gas-sensing performances of coral-like SnO_2–CuO nanocomposite. Acta Metall Sin (Engl Lett) 28:1190–1197

[8] Lee J-H, Kim J-H, Kim SS (2018) CuO–TiO_2 p–n core-shell nanowires: sensing mechanism and p/n sensing-type transition. Appl Surf Sci 448:489–497

[9] Ramgir NS, Ganapathi SK, Kaur M, Datta N, Muthe KP, Aswal DK, Gupta SK, Yakhmi JV (2010) Sub-ppm H_2S sensing at room temperature using CuO thin films. Sens Actuators B Chem 151:90–96

[10] Seyama M, Iwasaki Y, Ogawa S, Sugimoto I, Tate A, Niwa O (2005) Discriminative detection of volatile sulfur compound mixtures with a plasma-polymerized film-based sensor array installed in a humidity-control system. Anal Chem 77:4228–4234

[11] Kramer KE, Rose-Pehrsson SL, Hammond MH, Tillett D, Streckert HH (2007) Detection and classification of gaseous sulfur compounds by solid electrolyte cyclic voltammetry of cermet sensor array. Anal Chim Acta 584:78–88

[12] Mironenko AY, Sergeev AA, Nazirov AE, Modin EB, Voznesenskiy SS, Bratskaya SY (2016) H_2S optical waveguide gas sensors based on chitosan/Au and chitosan/Ag nanocomposites. Sens Actuators B Chem 225:348–353

[13] Yang M, Sun Y, Zhang D, Jiang D (2010) Using Pd/WO_3 composite thin films as sensing materials for optical fiber hydrogen sensors. Sens Actuators B Chem 143:750–753

[14] Lee Y-S, Joo B-S, Choi N-J, Lim J-O, Huh J-S, Lee D-D (2003) Visible optical sensing of ammonia based on polyaniline film. Sens Actuators B Chem 93:148–152

[15] Pandey SK, Kim K-H, Tang K-T (2012) A review of sensor-based methods for monitoring hydrogen sulfide. TrAC Trends Anal Chem 32:87–99

[16] Jagadale SB, Patil VL, Vanalakar SA, Patil PS, Deshmukh HP (2018) Preparation, characterization of 1D ZnO nanorods and their gas sensing properties. Ceram Int 44:3333–3340

[17] Zhu L, Li Y, Zeng W (2018) Hydrothermal synthesis of hierarchical flower-like ZnO nanostructure and its enhanced ethanol gas-sensing properties. Appl Surf Sci 427:281–287

[18] Yang X, Zhang S, Yu Q, Zhao L, Sun P, Wang T, Liu F, Yan X, Gao Y, Liang X, Zhang S, Lu G (2019) One step synthesis of branched SnO_2/ZnO heterostructures and their enhanced gas-sensing properties. Sens Actuators B Chem 281:415–423

[19] Zhong X, Shen Y, Zhao S, Chen X, Han C, Wei D, Fang P, Meng D (2019) SO_2 sensing properties of SnO_2 nanowires grown on a novel diatomite-based porous substrate. Ceram Int 45:2556–2565

[20] Zhou Q, Chen W, Xu L, Kumar R, Gui Y, Zhao Z, Tang C, Zhu S (2018) Highly sensitive carbon monoxide (CO) gas sensors based on Ni and Zn doped SnO_2 nanomaterials. Ceram Int 44:4392–4399

[21] Zhou Q, Xu L, Umar A, Chen W, Kumar R (2018) Pt nanoparticles decorated SnO_2 nanoneedles for efficient CO gas sensing applications. Sens Actuators B Chem 256:656–664

[22] Gao X, Zhou Q, Lu Z, Xu L, Zhang Q, Zeng W (2019) Synthesis of Cr_2O_3 nanoparticle-Coated SnO_2 nanofibers and C_2H_2 sensing properties. Front Mater 6:163

[23] Ding M, Xie N, Wang C, Kou X, Zhang H, Guo L, Sun Y, Chuai X, Gao Y, Liu F, Sun P, Lu G (2017) Enhanced NO_2 gas sensing properties by Ag-doped hollow urchin-like In_2O_3 hierarchical nanostructures. Sens Actuators B Chem 252:418–427

[24] Gu F, Nie R, Han D, Wang Z (2015) In_2O_3–graphene nanocomposite based gas sensor for selective detection of NO_2 at room temperature. Sens Actuators B Chem 219:94–99

[25] Kulkarni SB, Navale YH, Navale ST, Stadler FJ, Ramgir NS, Patil VB (2019) Hybrid polyaniline-WO_3 flexible sensor: a room temperature competence towards NH_3 gas. Sens Actuators B Chem 288:279–288

[26] Zappa D, Galstyan V, Kaur N, Hashitha MM, Arachchige M, Sisman O, Comini E (2018) Metal oxide-based heterostructures for gas sensors—a review. Anal Chim Acta 1039:1–23

[27] Umar A, Alshahranic AA, Algarnic H, Kumard R (2017) CuO nanosheets as potential scaffolds for gas sensing applications. Sens Actuators B Chem 250:24–31

[28] Diao K, Zhou M, Zhang J, Tang Y, Wang S, Cui X (2015) High response to H_2S gas with facile synthesized hierarchical ZnO microstructures. Sens Actuators, B 219:30–37

[29] Ayesh AI, Ahmed RE, Al-Rashid MA, Alarrouqi RA, Saleh B, Abdulrehman T, Haik Y, Al-Sulaiti LA (2018) Selective gas sensors using graphene and CuO nanorods. Sens Actuators A Phys 283:107–112

[30] Xu J, Li S, Li L, Chen L, Zhu Y (2018) Facile fabrication and superior gas sensing properties of spongelike Co-doped ZnO microspheres for ethanol sensors. Ceram Int 44:16773–16780

[31] Uddin ASMI, Yaqoob U, Phan D-T, Chung G-S (2016) A novel flexible acetylene gas sensor based on PI/PTFE-supported Ag-loaded vertical ZnO nanorods array. Sens Actuators B Chem 222:536–543

[32] Wang Y, Meng X, Yao M, Sun G, Zhang Z (2019) Enhanced CH_4 sensing properties of Pd modified ZnO nanosheets. Ceram Int 45(10):13150–13157

[33] Nancy Anna Anasthasiya A, Kampara RK, Rai PK, Jeyaprakash BG (2018) Gold functionalized ZnO nanowires as a fast response/recovery ammonia sensor. Appl Surf Sci 449:244–249

[34] Wang J, Zhou Q, Zeng W (2019) Competitive adsorption of SF_6 decompositions on Ni-doped ZnO (100) surface:

computational and experimental study. Appl Surf Sci 479:185–197

[35] Da Silva LF, M'Peko J-C, Catto AC, Bernardini S, Mastelaro VR, Aguir K, Ribeirod C, Longo E (2017) UV-enhanced ozone gas sensing response of ZnO–SnO_2 heterojunctions at room temperature. Sens Actuators B Chem 240:573–579

[36] Yang T, Gu K, Zhu M, Lu Q, Zhai C, Zhao Q, Yang X, Zhang M (2019) ZnO–SnO_2 heterojunction nanobelts: synthesis and ultraviolet light irradiation to improve the triethylamine sensing properties. Sens Actuators B Chem 279:410–417

[37] Lu Z, Zhou Q, Wang C, Wei Z, Xu L, Gui Y (2018) Electrospun ZnO–SnO_2 composite nanofibers and enhanced sensing properties to SF6 decomposition byproduct H_2S. Front Chem 6:540

[38] San X, Li M, Liu D, Wang G, Shen Y, Meng D, Meng F (2018) A facile one-step hydrothermal synthesis of NiO/ZnO heterojunction microflowers for the enhanced formaldehyde sensing properties. J Alloys Compd 739:260–269

[39] Zhou Q, Zeng W, Chen W, Xu L, Kumar R, Umar A (2019) High sensitive and low-concentration sulfur dioxide (SO_2) gas sensor application of heterostructure NiO–ZnO nanodisks. Sens Actuators B Chem 298:126870

[40] Runa A, Zhang X, Wen G, Zhang B, Fu W, Yang H (2018) Actinomorphic flower-like n-ZnO/p-$ZnFe_2O_4$ composite and its improved NO_2 gas-sensing property. Mater Lett 225:73–76

[41] Choi SW, Katoch A, Kim JH, Kim SS (2014) Prominent reducing gas-sensing performances of n-SnO_2 nanowires by local creation of p–n heterojunctions by functionalization with p-Cr_2O_3 nanoparticles. ACS Appl Mater Interface 6:17723–17729

[42] Wang ZL (2008) Splendid one-dimensional nanostructures of zinc oxide: a new nanomaterial family for nanotechnology. ACS Nano 2:1987–1992

[43] Zhang Y, Liu Y, Zhou L, Liu D, Liu F, Liu F, Liang X, Yan X, Gao Y, Lu G (2018) The role of Ce doping in enhancing sensing performance of ZnO-based gas sensor by adjusting the proportion of oxygen species. Sens Actuators B Chem 273:991–998

[44] Zhu L, Zeng W (2017) Room-temperature gas sensing of ZnO-based gas sensor: a review. Sens Actuators, A 267:242–261

[45] Iwamoto M, Yoda Y, Yamazoe N, Seiyama T (1978) Study of metal oxide catalysts by temperature programmed desorption. 4. Oxygen adsorption on various metal oxides. J Phys Chem C 82:2564–2570

[46] Kim H-J, Lee J-H (2014) Highly sensitive and selective gas sensors using p-type oxide semiconductors: overview. Sens Actuators B Chem 192:607–627

[47] Park S, Kim S, Kheel H, Hyun SK, Jin C, Lee C (2016) Enhanced H_2S gas sensing performance of networked CuO–ZnO composite nanoparticle sensor. Mater Res Bull 82:130–135

[48] Datta N, Ramgir NS, Kumar S, Veerender P, Kaur M, Kailasaganapath S, Debnath AK, Aswal DK, Gupta SK (2014) Role of various interfaces of CuO/ZnO random nanowire networks in H_2S sensing: an impedance and Kelvin probe analysis. Sens Actuators B Chem 202:1270–1280

[49] Zhang Y-B, Yin J, Li L, Zhang L-X, Bie L-J (2014) Enhanced ethanol gas-sensing properties of flower-like p-CuO/n-ZnO heterojunction nanorods. Sens Actuators B Chem 202:500–507

[50] Diao K, Xiao J, Zheng Z, Cui X (2018) Enhanced sensing performance and mechanism of CuO nanoparticle-loaded ZnO nanowires: comparison with ZnO–CuO core-shell nanowires. Appl Surf Sci 459:630–638

[51] Liu X, Du B, Sun Y, Yu M, Yin Y, Tang W, Chen C, Sun L, Yang B, Cao W, Ashfold MN (2016) Sensitive room temperature photoluminescence-based sensing of H_2S with novel CuO–ZnO nanorods. ACS Appl Mater Interface 8:16379–16385

[52] Li D, Qin L, Zhao P, Zhang Y, Liu D, Liu F, Kang B, Wang Y, Song H, Zhang T, Lu G (2018) Preparation and gas-sensing performances of ZnO/CuO rough nanotubular arrays for low-working temperature H_2S detection. Sens Actuators B Chem 254:834–841

[53] Katoch A, Choi S-W, Kim J-H, Lee JH, Lee J-S, Kim SS (2015) Importance of the nanograin size on the H_2S-sensing properties of ZnO–CuO composite nanofiber. Sens Actuators, B 214:111–116

[54] Kim J-H, Lee J-H, Mirzaei A, Kim HW, Kim SS (2017) Optimization and gas sensing mechanism of n-SnO_2-p-Co_3O_4 composite nanofiber. Sens Actuators, B 248:500–511

[55] Kim J-H, Lee J-H, Mirzaei A, Kim HW, Kim SS (2018) SnO_2 (n)-NiO (p) composite nanowebs: gas sensing properties andsensing mechanisms. Sens Actuators, B 258:204–214

[56] Yan C, Lu H, Gao J, Zhu G, Yin F, Yang Z, Liu Q, Li G (2017) Synthesis of porous NiO–In_2O_3 composite nanofibers by electrospinning and their highly enhanced gas sensing properties. J Alloys Compd 699:567–574

[57] Wang L, Kang Y, Wang Y, Zhu B, Zhang S, Huang W, Wang S (2012) CuO nanoparticle decorated ZnO nanorod sensor for low-temperature H_2S detection. Mater Sci Eng, C 32:2079–2085

[58] Park S, Park S, Jung J, Hong T, Lee S, Kim HW, Lee C (2014) H_2S gas sensing properties of CuO-functionalized WO_3 nanowires. Ceram Int 40:11051–11056

[59] Kim H, Jin C, Park S, Kim S, Lee C (2012) H_2S gas sensing properties of bare and Pd-functionalized CuO nanorods. Sens Actuators B Chem 161:594–599

[60] Wang M, Luo Q, Hussain S, Liu G, Qiao G, Kim EJ (2019) Sharply-precipitated spherical assembly of ZnO nanosheets for low temperature H_2S gas sensing performances. Mater Sci Semicond Process 100:283–289

[61] Guoa W, Li X, Qin H, Wang Z (2015) PEG-20000 assisted hydrothermal synthesis of hierarchical ZnO flowers: structure, growth and gas sensor properties. Phys E 73:163–168

[62] Zhang B, Liu G, Cheng M, Gao Y, Zhao L, Li S, Liu F, Yan X, Zhang T, Sun P, Lu G (2018) The preparation of reduced graphene oxide-encapsulated α-Fe_2O_3 hybrid and its outstanding NO_2 gas sensing properties at room temperature. Sens Actuators B Chem 261:252–263

[63] Qin C, Wang Y, Gong Y, Zhang Z, Cao J (2019) CuO–ZnO hetero-junctions decorated graphitic carbon nitride hybrid nanocomposite: hydrothermal synthesis and ethanol gas sensing application. J Alloys Compd 770:972–980

[64] Vasiliev RB, Rumyantseva MN, Yakovlev NV, Gaskov AM (1998) CuO/SnO_2 thin film heterostructures as chemical sensors to H_2S. Sens Actuators, B 50:186–193

[65] Hu X, Zhu Z, Li Z, Xie L, Wu Y, Zheng L (2018) Heterostructure of CuO microspheres modified with $CuFe_2O_4$ nanoparticles for highly sensitive H_2S gas sensor. Sens Actuators B Chem 264:139–149

[66] Choi S-W, Katoch A, Zhang J, Kim SS (2013) Electrospun nanofibers of CuO–SnO_2 nanocomposite as semiconductor gas sensors for H_2S detection. Sens Actuators B Chem 176:585–591

[67] Katoch A, Kim J-H, Kim SS (2015) Significance of the nanograin size on the H_2S-sensing ability of CuO–SnO_2 composite nanofibers. J Sens 2015:1–7

[68] Khalil A, Kim JJ, Tuller HL, Rutledge GC, Hashaikeh R (2016) Gas sensing behavior of electrospun nickel oxide nanofibers: effect of morphology and microstructure. Sens Actuators B Chem 227:54–64

[69] Zhang L, Jiao W (2015) The effect of microstructure on the gas properties of $NiFe_2O_4$ sensors: nanotube and nanoparticle. Sens Actuators B Chem 216:293–297